IJMMM International Journal of Minerals, Metallurgy and Materials 矿物冶金与材料学报（英文版）

Phase changes and electromagnetic wave absorption performance of XZnC (X = Fe/Co/Cu) loaded on melamine sponge hollow carbon composites

Xiubo Xie, Ruilin Liu, Chen Chen, Di Lan, Zhelin Chen, Wei Du, and Guanglei Wu

Cite this article as:
Xiubo Xie, Ruilin Liu, Chen Chen, Di Lan, Zhelin Chen, Wei Du, and Guanglei Wu, Phase changes and electromagnetic wave absorption performance of XZnC (X = Fe/Co/Cu) loaded on melamine sponge hollow carbon composites, *Int. J. Miner. Metall. Mater.*, 32(2025), No. 3, pp. 566-577. https://doi.org/10.1007/s12613-024-3024-3

View the article online at SpringerLink or IJMMM Webpage.

INTERNATIONAL JOURNAL OF
Minerals, Metallurgy and Materials

Volume 32, Number 3, March 2025
Page 566

Research Article https://doi.org/10.1007/s12613-024-3024-3

Phase changes and electromagnetic wave absorption performance of XZnC (X = Fe/Co/Cu) loaded on melamine sponge hollow carbon composites

Xiubo Xie[1),*,✉], *Ruilin Liu*[1),*], *Chen Chen*[1),*], *Di Lan*[2)], *Zhelin Chen*[1)], *Wei Du*[1,3),✉], *and Guanglei Wu*[4),✉]

1) School of Environmental and Material Engineering, Yantai University, Yantai 264005, China
2) School of Materials Science and Engineering, Hubei University of Automotive Technology, Shiyan 442002, China
3) Shandong Key Laboratory of Eco-Environmental Science for the Yellow River Delta, Shandong University of Aeronautics, Binzhou 256603, China
4) Institute of Materials for Energy and Environment, State Key Laboratory of Bio-fibers and Eco-textiles, College of Materials Science and Engineering, Qingdao University, Qingdao 266071, China

(Received: 21 July 2024; revised: 8 October 2024; accepted: 11 October 2024)

Abstract: Non-stoichiometric carbides have been proven to be effective electromagnetic wave (EMW) absorbing materials. In this study, phase and morphology of XZnC (X = Fe/Co/Cu) loaded on a three dimensional (3D) network structure melamine sponge (MS) carbon composites were investigated through vacuum filtration followed by calcination. The FeZnC/CoZnC/CuZnC with carbon nanotubes (CNTs) were uniformly dispersed on the surface of melamine sponge carbon skeleton and Co-containing sample exhibits the highest CNTs concentration. The minimum reflection loss (RL_{min}) of the CoZnC/MS composite ($m_{composite}$: $m_{paraffin}$ = 1:1, m represents mass) reached −33.60 dB, and the effective absorption bandwidth (EAB) reached 9.60 GHz. The outstanding electromagnetic wave absorption (EMWA) properties of the CoZnC/MS composite can be attributed to its unique hollow structure, which leads to multiple reflections and scattering. The formed conductive network improves dielectric and conductive loss. The incorporation of Co enhances the magnetic loss capability and optimizes interfacial polarization and dipole polarization. By simultaneously improving dielectric and magnetic losses, excellent impedance matching performance is achieved. The clarification of element replacement in XZnC/MS composites provides an efficient design perspective for high-performance non-stoichiometric carbide EMW absorbers.

Keywords: electromagnetic wave absorption; three dimensional network structure; melamine sponge derived carbon; non-stoichiometric carbide

1. Introduction

The accelerated advancement of contemporary technology has led to the widespread use of various electronic devices, resulting in significant electromagnetic (EM) pollution [1–3]. The pollution not only causes electromagnetic interference with electronic equipment but also poses substantial harm to the human health [4]. Consequently, addressing electromagnetic pollution has emerged as a pressing concern [5]. To safeguard human health and electronic devices, the development of electromagnetic wave (EMW) absorbing materials is crucial. The materials are used to dissipate incident EWM or convert them into heat through interference effects, offering an effective solution to electromagnetic radiation and interference issues [6]. Currently, research on enhancing electromagnetic wave absorption (EMWA) performance has seen a significant progress in studies focusing on metal carbide materials [7–12]. In the past decades, the well-known magnetic metal carbides include Fe_3C [13], Ni_3C [14], and Co_3ZnC [15]. Although these materials possess dielectric loss and magnetic loss with multiple loss mechanisms optimized for impedance matching, as well as good electrical conductivity, thermal and chemical stability, resulting in improved electromagnetic wave absorption performance, their ability to provide heterogeneous interfaces and defects as stoichiometric ratio compounds is limited. Thus it is also constrained to fulfil the requirements of strong absorption, wide bandwidth and minimum thickness [16]. Among the various materials, $Ni_3ZnC_{0.7}$ and its composite counterparts have increasingly become a focal point of research. The EMWA properties of the composite materials have been significantly enhanced. Qi *et al.* [17] reported that the $Ni_3ZnC_{0.7}$/CNTs (carbon nanotubes)/melamine sponge (MS) carbon composite (filtrating time of 2 h) exhibited the minimum reflection loss (RL_{min}) value of −114.5 dB (1.3 mm) and an effective absorption bandwidth (EAB) of 12.5 GHz at a matching thickness of 1.9 mm. Ding *et al.* [18] embedded bimetallic transition carbide nanoparticles $Ni_3ZnC_{0.7}$ in nitrogen-rich layered porous carbon nanosheets, and the RL_{min} value of the composite was −69.1 dB at 12.7 GHz, and the

*These authors contributed equally to this work

✉ Corresponding authors: Xiubo Xie E-mail: xiuboxie@ytu.edu.cn; Wei Du E-mail: duwei@ytu.edu.cn;
Guanglei Wu E-mail: wuguanglei@qdu.edu.cn

Springer

EAB was 6.5 GHz. Sun *at al*. [19] researched the RL_{min} value of the $Ni_3ZnC_{0.7}$/Ni loaded puffed-rice derived carbon composite reaches −39.9 dB at 8.6 GHz, while the widest EAB of the composite can reach 9.9 GHz (8.1–18 GHz, 1.49 mm).

In this work, the element Ni of $Ni_3ZnC_{0.7}$ was substituted with various elements (Fe, Co, Cu). The substitutions were made on the surface of a three dimensional (3D) skeleton using both the sol–gel method and the immersion method, with the aim of preparing composites exhibiting different magnetic phases. FeZnC, CoZnC, and CuZnC precursors were calcined under nitrogen atmosphere to obtain FeZnC/MS, CoZnC/MS, and CuZnC/MS composites. A comparative analysis was conducted on the morphology, structure, and EMWA performance of FeZnC/MS, CoZnC/MS, and CuZnC/MS composites. As anticipated, the composites loaded with Fe, Co, and Zn all yielded sponge skeleton-loaded particles and carbon nanotubes. However, when compared to Fe and Cu, the CoZnC composites demonstrated superior EMWA properties. The optimized impedance matching resulted in effective attenuation of the composites. The spongy hollow carbon exhibits excellent impedance matching with free air, significantly increasing the number of solid–air interfaces and thereby enhancing EMWA performance. The inherent benefits of spongy hollow carbon, including its lightweight nature, large specific surface area, and adjustable dielectric loss, are further underscored. The experimental concept of substituting Ni with various metal elements is validated, yielding an EAB absorbing material of superior performance. This discovery offers a novel research approach for the exploration of other metal absorbing materials.

2. Experimental

2.1. Preparation of FeZnC/MS, CoZnC/MS, and CuZnC/MS materials

Instead of nickel acetate, iron acetate, cobalt acetate and copper acetate were used as raw materials, respectively. 11.25 mmol of ferric acetate (cobalt acetate, copper acetate) and 3.75 mmol of zinc acetate were dispersed into 125 mL of N,N-dimethylformamide (DMF) and stirred for 30 min to obtain liquid A. Meanwhile, 9 mmol of terephthalic acid (PTA) and 2.125 mL of triethylamine (TEA) were dispersed into 100 mL of DMF and stirred for 30 min to obtain liquid B. Then liquid B was poured into liquid A and continued to be stirred for 1 h to obtain FeZnC (CoZnC, CuZnC) precursor solution. The precursor solution and MS were poured into a filter for filtration, and after 1 h, the sample was taken out and put into a tube furnace to 700°C at a heating rate of 5°C·min^{-1} at the N_2 atmosphere, and then annealed for 10 h to obtain the FeZnC/MS, CoZnC/MS, and CuZnC/MS composites. The synthesis process of FeZnC/MS, CoZnC/MS, and CuZnC/MS is shown in Fig. 1.

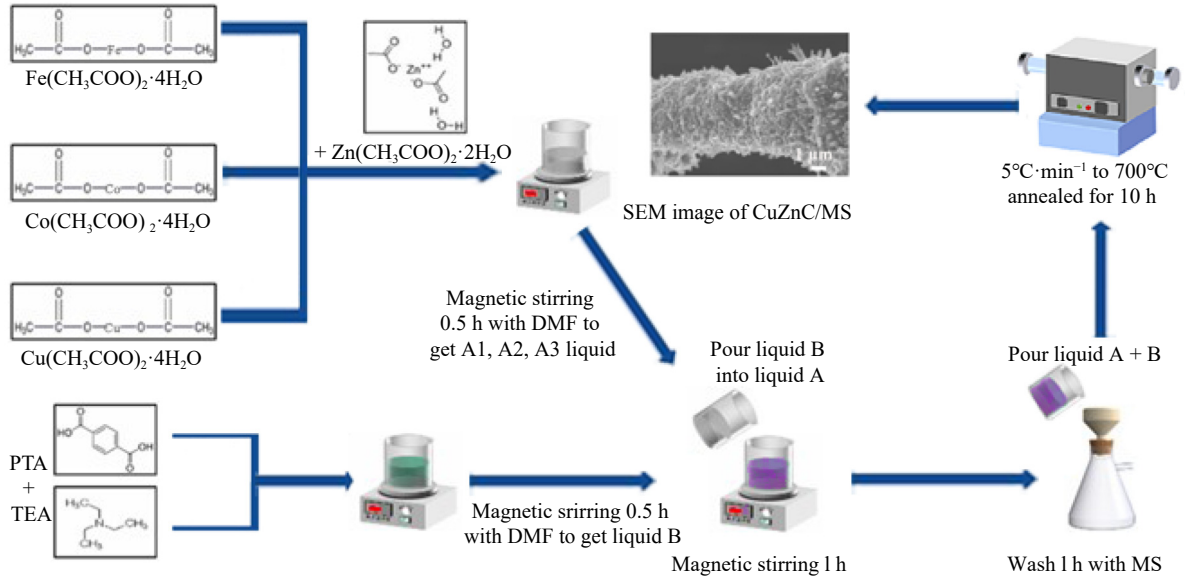

Fig. 1. Schematic of the preparation of FeZnC/MS, CoZnC/MS, and CuZnC/MS composites. SEM: scanning electron microscopy.

2.2. Characterizations

The phase, morphology and structure of the FeZnC/MS, CoZnC/MS, and CuZnC/MS samples were observed by X-ray diffraction (XRD) and scanning electron microscopy (SEM). Raman spectrometer was applied to determine the graphitization degree. Thermo Fisher ESCALAB 250Xi spectrometer (Al K_α X-ray source) was designed to get the X-ray photoelectron spectroscopy (XPS) curves. Electromagnetic measurements of FeZnC/MS, CoZnC/MS, and CuZnC/MS toroidal rings were studied by vector network analyzer (VAN, 3656D). According to the transmission line theory, the RL values were made by Eqs. (1) and (2) [20–21]:

$$Z_{in} = Z_0 \sqrt{\frac{\mu_r}{\varepsilon_r}} \tanh\left(j\frac{2\pi f d}{c}\sqrt{\mu_r \varepsilon_r}\right) \quad (1)$$

$$RL = 20\lg\left|\frac{(Z_{in} - Z_0)}{(Z_{in} + Z_0)}\right| \quad (2)$$

where Z_{in}, c, and Z_0 represent the input impedance, velocity, and impedance of the absorber in free space, respectively, μ_r, ε_r, and j represent complex permeability, complex permittiv-

ity, and imaginary unit, respectively, f is the frequency of the microwaves, and d should be the thickness of the absorber.

3. Results and discussion

3.1. Structural characterization

The XRD spectra of the synthesized samples are shown in Fig. 2. The sharp diffraction peak at 44.7° and two small diffraction peaks at 63.1° and 82.4° are shown in Fig. 2(a), matching well with the (110), (200) and (211) lattice planes of Fe (JCPDS No. 06-0696) [22]. In addition, characteristic peaks of metal carbides such as FeC, Fe_2C, etc. are also presented. The diffraction peaks at 43.9°, 52.1°, and 77.6° in Fig. 2(b) can be pointed to the (113), (300) lattice planes of monomeric Co (JCPDS No. 15-0806) [23]. The characteristic peaks at 42.8° and 51.3° in Fig. 2(c) can be attributed to the (111), (220), and (311) lattice planes of Cu (JCPDS No. 04-0836) [24]. From the XRD results it can be seen that the main magnetic components are stemmed from the Fe, Co, and Cu after the substitution of different metal elements. Raman spectroscopy can be used to determine the degree of graphitisation of the material. The two Raman characteristic peaks at 1340 and 1580 cm^{-1} are attributed to disordered carbon (D band) and ordered carbon (G band), respectively (Fig. 2(d)–(f)). The D band and G band are correspondingly related to the vibrational modes of defects and sp^2 carbon atoms [25]. It can be observed that the I_D/I_G (D peak value divided by G peak value) values of FeZnC, CoZnC, and CuZnC are close to each other, and thus the graphitizing degree is similar.

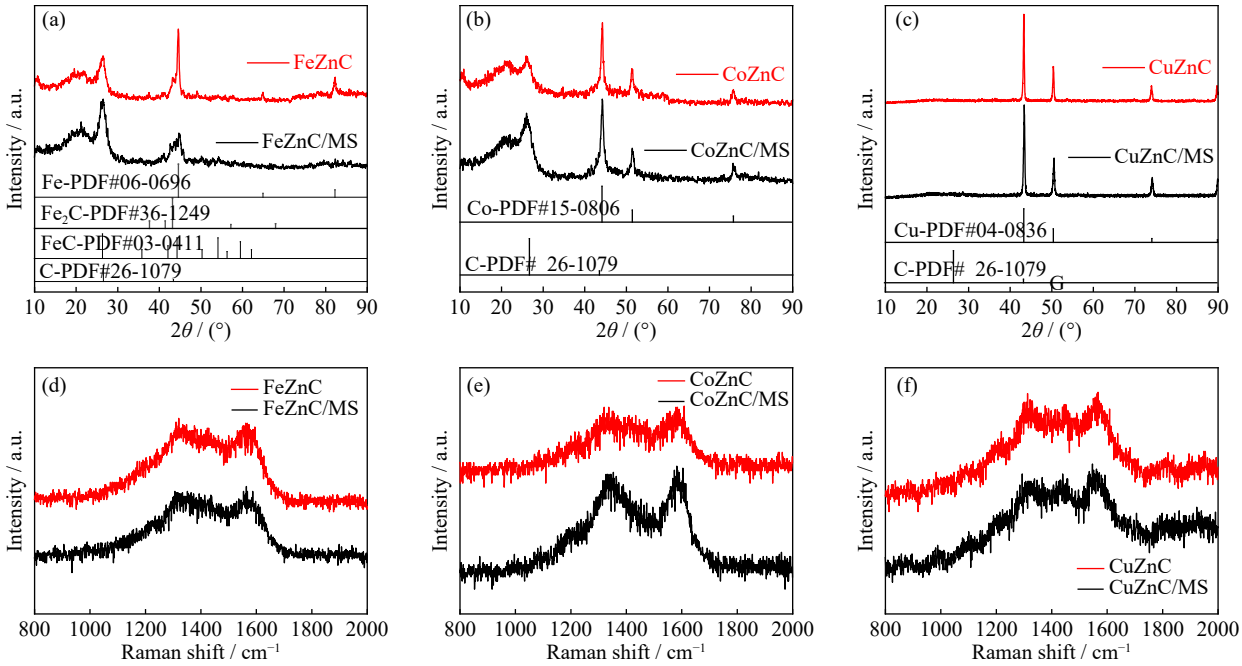

Fig. 2. (a–c) XRD and (d–e) Raman images of the FeZnC/MS, CoZnC/MS, and CuZnC/MS.

It can be seen from SEM images that all the three groups of samples exhibit a typical 3D network structure, where the sponge skeleton consists of microtubes with an average diameter of 3 μm and hollow spherical shell structures with a diameter of 15 μm, with carbon nanotubes as well as metal particles growing on the surface (Fig. 3). The Co particles are loaded on the sponge skeleton and catalyse the formation of a large number of carbon nanotubes which are uniformly distributed on the surface of the sponge skeleton, forming a rich interfacial structure (Fig. 3(b1)–(b3)). For FeZnC/MS and CuZnC/MS, the skeletal structure remains unchanged. Although carbon nanotubes were also catalytically generated, their number is significantly less than that of CoZnC/MS, suggesting that the catalytic activity of Co surpasses that of Fe and Cu. In fact, carbon nanotubes were not obviously generated in the CuZnC system, which showed a heterogeneous structure of Cu particles bonded to carbon instead (Fig. 3(c3)). On the one hand, the electronic structure of cobalt atoms makes them highly active in catalyzing the decomposition of carbon source. They can effectively promote the cleavage of carbon source molecules to generate free carbon atoms. These free carbon atoms can subsequently recombine under appropriate conditions to form carbon nanotubes [26]. During the catalysis process, cobalt nanoparticles can provide good growth sites and facilitate the directional growth of carbon nanotubes. In contrast, copper has a lower catalytic activity and is less likely to effectively cleave carbon source molecules. The interaction force between catalyst and carbon atoms is also very important for the growth of carbon nanotubes. The weak interaction force between copper and carbon atoms is not conducive to the migration and reassembly of carbon atoms. On the other hand, besides the existence of iron, detectable amount of Fe_2C and FeC can decrease the catalytic activity of the iron.

Transmission electron microscope (TEM) was used to further characterise the micro-morphology and lattice information of the material as shown in Fig. 4. Fig. 4(a) and (b) shows the low resolution TEM image with a large number of

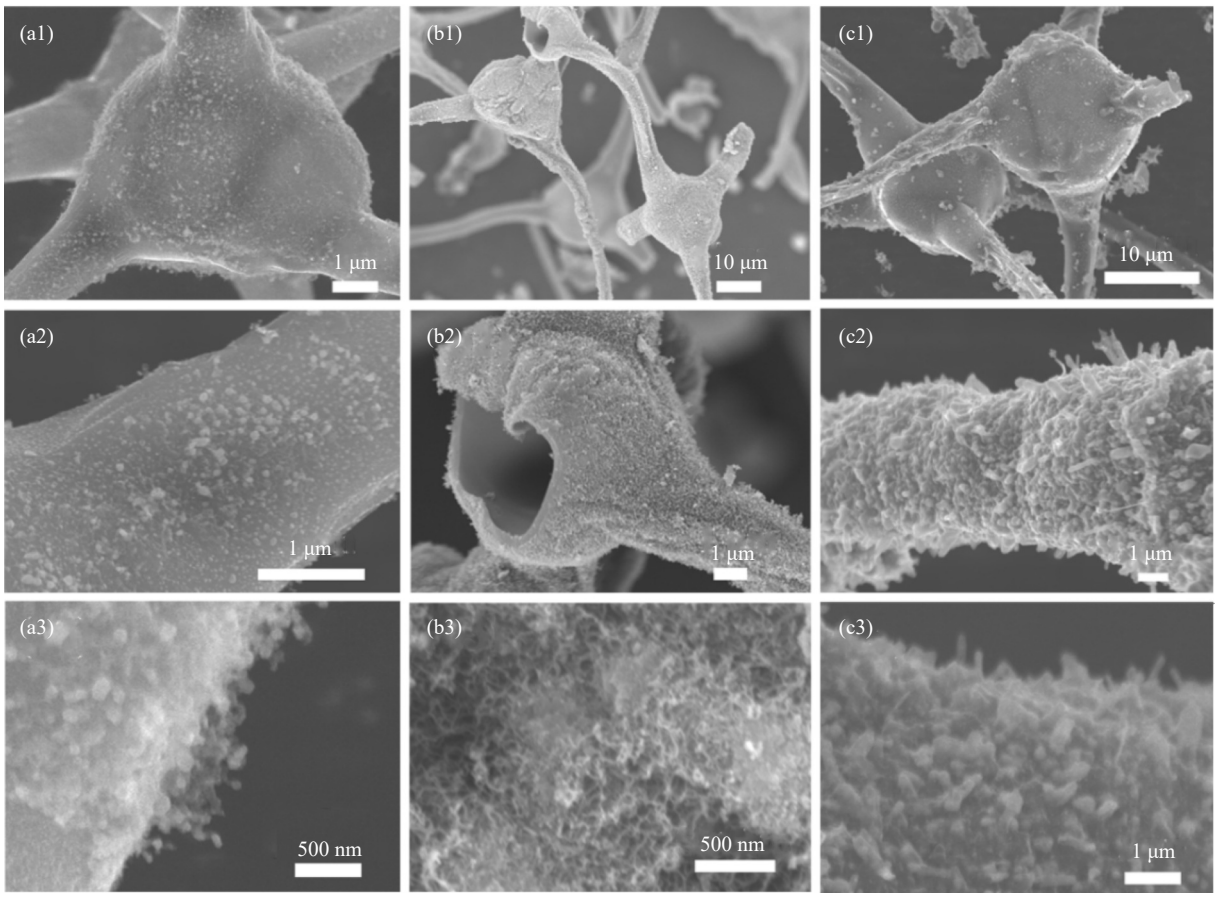

Fig. 3. SEM images of (a1–a3) FeZnC/MS, (b1–b3) CoZnC/MS, and (c1–c3) CuZnC/MS from low to high resolution.

carbon nanotube structures on the surface of the CoZnC/MS sample and nanoparticles wrapped around the nanotube beginnings. It is further observed from the high resolution TEM image (Fig. 4(c) and (d)) that the nanoparticles have a lattice plane spacing of 0.176 nm, which can be indexed to the (200) lattice plane of Co, suggesting that the nanoparticles wrapped around the tip of the nanotubes are Co monomers. The nanotubes surrounding the Co particles correspond to the C element. Based on energy dispersive spectrometer (EDS) mapping results, C (red region), Co (yellow region) and Zn (green region) elements were uniformly distributed in CoZnC/MS (Fig. 4(f)–(h)). TEM analysis verified the successful preparation of CoZnC/MS composites as well as the important role of Co particles on the formation of carbon nanotubes.

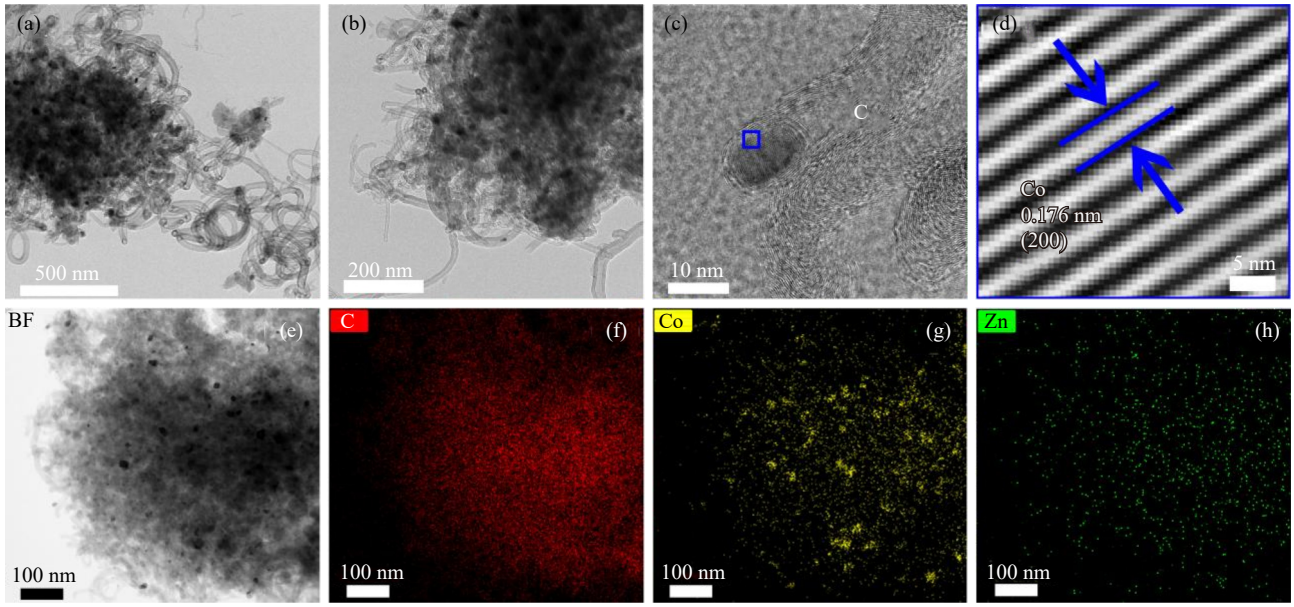

Fig. 4. (a, b) TEM, (c, d) high resolution TEM images, and (e–h) corresponding C, Co, and Zn EDS maps of CoZnC/MS composites.

The surface chemical compositions of Fe (Co, Cu) ZnC/MS materials were further investigated by XPS, as shown in Fig. 5. Based on the full XPS spectra of the three composites (Fig. 5(a)), the C, O, N, Fe (Cu, Co), and Zn elements on the surfaces of the three groups of samples were analysed and compared one by one. For the N 1s spectra (Fig. 5(b)), the N 1s spectra was fitted as three different peaks at about 398.2, 400.7, and 406.7 eV, representing pyridinic-N, graphitic-N, and oxidized-N, respectively [27]. In this work, triethylamine was used as a nitrogen-containing ligand, with the nitrogen contained in the carbon material itself as the source. For the O 1s spectra (Fig. 5(c)), the O 1s spectra have two different peaks at about 529.7, 531.9 eV, representing –OH, –COOH, respectively [28]. In addition, the characteristic peak of CoZnC/MS sample at 533.6 eV corresponds to C–O peak and FeZnC/MS sample at 530.3 eV corresponds to C=O peak [29]. The C 1s spectra show similar spectra with three major peaks at 289.1, 286.7, and 284.8 eV, which corresponds to C=O, C–N, and C=C, respectively (Fig. 5(d)) [30–31]. It can be observed in Fig. 5(f) that the Fe 2p spectrum consisting of six peaks is attributed to Fe^0 (710.6 and 724.8 eV), Fe^{2+} (713.1 and 726.7 eV), and satellite peaks (719.2 and 733.8 eV) [32]. The Co 2p spectra were combined by Co^0 (779.6 and 794.9 eV), Co^{2+} (781.2 and 796.3 eV), and satellite peaks (788.3 and 804.7 eV), respectively (Fig. 5(g)) [33]. On the other hand, the observed characteristic Cu 2p peaks at 931.5 and 943.8 eV are consistent with Cu^0, whereas the peaks at 935.3 and 954.7eV are associated with Cu^{2+} and the peaks at 942.8 and 963.1 eV belong to satellite peaks (Fig. 5(h)) [34].

3.2. Electromagnetic parameters and EMWA performance

Electromagnetic parameters play a key role in revealing the electromagnetic absorption properties of Fe (Co, Cu) ZnC/MS samples. The real (ε') and imaginary (ε'') parts of complex permittivity are shown in Fig. 6(a) and (b). The values of ε' and ε'' for FeZnC/MS are higher than that of CoZnC/MS and CuZnC/MS, which indicate that FeZnC/MS has a larger dielectric energy storage capacity and dissipation capability. FeZnC/MS has high ε'' values in the range of 2–4 GHz, which suggests that the material possesses a high

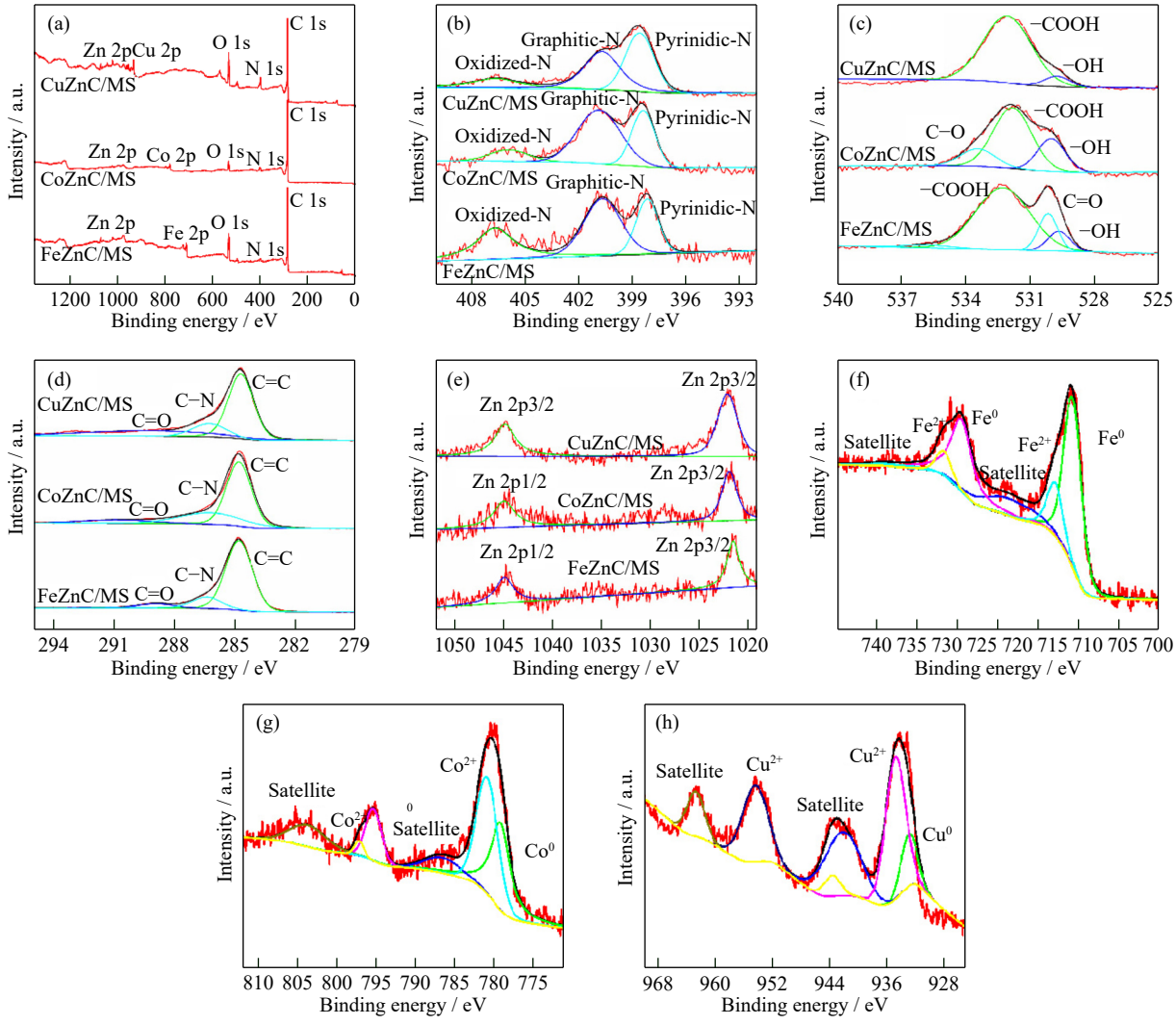

Fig. 5. (a) XPS full spectra, high-resolution XPS spectra of (b) N 1s, (c) O 1s, (d) C 1s, (e) Zn 2p of the FeZnC/MS, CoZnC/MS, and CuZnC/MS. High-resolution XPS spectra of (f) Fe 2p of the FeZnC/MS, (g) Co 2p of the CoZnC/MS, and (h) Cu 2p of the CuZnC/MS.

electrical conductivity, whereas too high conductivity leads to the EMW reflection at the surface of the absorber [35]. Therefore, the dielectric constant obtained for CoZnC/MS is rather more favourable for the absorption of EMW. The angular tangent of dielectric loss ($\tan\delta_\varepsilon = \varepsilon''/\varepsilon'$) of FeZnC/MS is higher than that of CoZnC/MS and CuZnC/MS at low frequencies, which suggests that FeZnC/MS has a stronger dielectric loss capability at low frequencies (Fig. 6(c)). The real (μ') and imaginary (μ'') parts of the complex permeability of Fe (Co, Cu) ZnC/MS samples are shown in Fig. 6(d) and (e). It can be clearly seen that the μ' and μ'' values of CuZnC/MS and FeZnC/MS are higher than that of the other two samples respectively, indicating that the CuZnC/MS has a better magnetic energy storage capacity, while FeZnC/MS has a better magnetic dissipation capacity. After comparison, the curve in Fig. 6(e) is located at the same place where the peak value of μ'' corresponds to the trough value in ε'', and the trend is also observed for μ'–ε' and $\tan\delta_\mu$($\tan\delta_\mu = \mu''/\mu'$)–$\tan\delta_\varepsilon$ in the mid-to-high frequency range. The phenomenon suggests that the complex permeability of the sample will respond to the dielectric transition, which may be due to electromagnetic coupling effects [36]. It can be seen that some imaginary part of permeability values are blew 0 for CuZnC/MS composite. According to Maxwell's equations, the highly conductive component (spongy carbon) of the composite promotes charge transfer and generates an internal magnetic field (Faraday's law of electromagnetic induction) in the presence of an alternating electromagnetic field. The presence of this internal magnetic field cancels out some of the magnetic losses generated by the composite as a whole, resulting in a negative value of μ'' [37]. At certain frequencies, the phase-delayed nature of the material may lead to a reverse flow of energy, which also contributes to the negative behaviour of the imaginary part of the magnetic permeability. For EMW absorbing materials, the values of $\tan\delta_\varepsilon$ and $\tan\delta_\mu = \mu''/\mu'$ can reflect their dielectric and magnetic losses to a certain extent, but cannot be proved to have excellent wave absorbing properties, since the impedance matching of the material must be satisfied firstly.

The 3D reflection maps and two dimensional (2D) RL of the three composites are shown in Fig. 7 when the filling ratio of the nanocomposites is 1:1. It can be clearly seen that the RL of CoZnC/MS composite (Fig. 7(b)) is better than that of FeZnC/MS (Fig. 7(a)) and CuZnC/MS (Fig. 7(c)) over the whole frequency range, which implies that the substitution of the Co element is more optimised for the EMWA performance. The result may be due to the richer microstructure growth on the surface of CoZnC/MS composites, which is conducive to the improvement of the impedance matching of the materials. The RL_{min} value of CoZnC/MS composite at 11.12 GHz is −33.60 dB (1.20 mm), and the corresponding EAB is 9.60 GHz (1.20 mm, 8.4–18.00 GHz). The RL_{min} values for FeZnC/MS and CuZnC/MS are −14.00 dB and −26.50 dB, respectively. In addition, the effect of different paraffin filling rates of the materials on the performance of EMWA is investigated (Figs. S1 and S2, see the Supplementary Information). Under the paraffin filling ratios of 1:2 and 1:3, the permittivity of the optimum sample CoZnC/MS is too large leading to the impedance mismatch of the material, and thus the performance is bad, and the RL values are all above −10 dB.

Fig. 8 shows a plot of the calculated RL versus frequency for all three samples at different thicknesses (1–3 mm). It is well known that when the RL is equal to −10 dB, the EMW absorption is considered to be 90%, and the frequency range where the RL is less than −10 dB is considered to be the

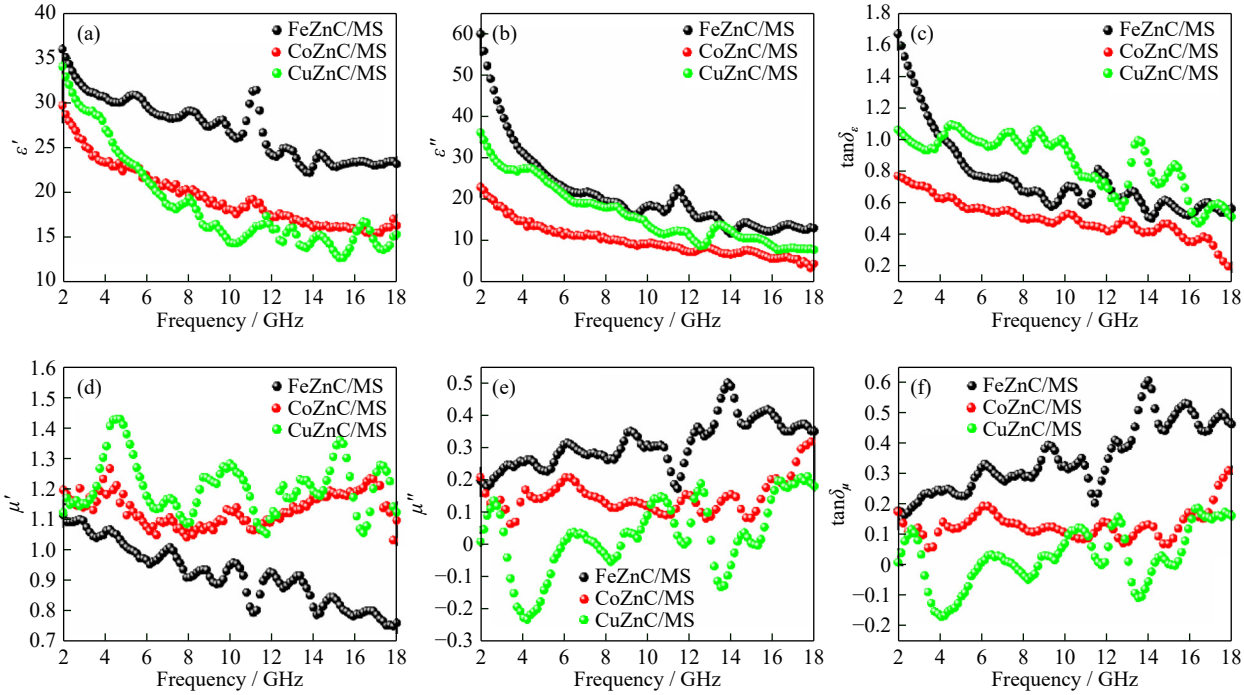

Fig. 6. (a) Real part, (b) imaginary part, and (c) $\tan\delta_\varepsilon$ of permittivity, (d) real part, (e) imaginary part, and (f) $\tan\delta_\mu$ of permeability of the FeZnC/MS, CoZnC/MS, and CuZnC/MS.

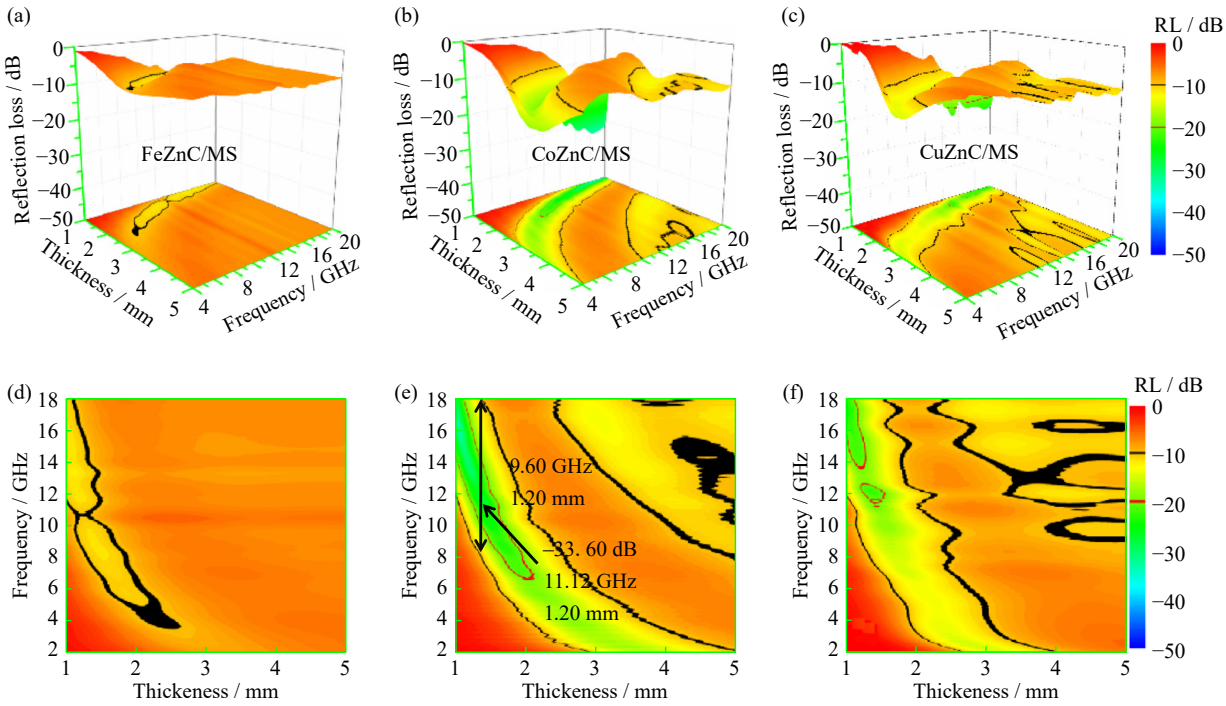

Fig. 7. 3D images and 2D images of calculated theoretical RL value of (a, d) FeZnC/MS, (b, e) CoZnC/MS , and (c, f) CuZnC/MS.

EAB. From the RL curves of the three samples, it can be seen that the EMWA ability of FeZnC/MS and CuZnC/MS is relatively weak. For CoZnC/MS, the dissipation ability to the incident EMW is improved. The RL_{min} is as low as −32.70 dB for a matched thickness of only 1 mm, which gives the material a significant advantage for practical applications. The impedance matching ($|Z_{in}/Z_0|$) curves of FeZnC/MS, CoZnC/MS, and CuZnC/MS composites with different thicknesses are calculated and the results are shown in Fig. 8(a2)–(c2). The closer the value of $|Z_{in}/Z_0|$ is to 1, the better the impedance matching between the absorber and the EMW, which means that more EMW enters into the absorber and attenuates it. As a result of the magnetic nanoparticles and carbon nanotubes optimise the magnetic and dielectric losses, the $|Z_{in}/Z_0|$ curves show that CoZnC/MS is better than FeZnC/MS and CuZnC/MS. CoZnC/MS has better impedance matching than FeZnC/MS and CuZnC/MS.

In general, the dielectric loss consists of dipole polarization and interface polarization within the EMW band. The multiple semicircles indicate the presence of multiple polar-

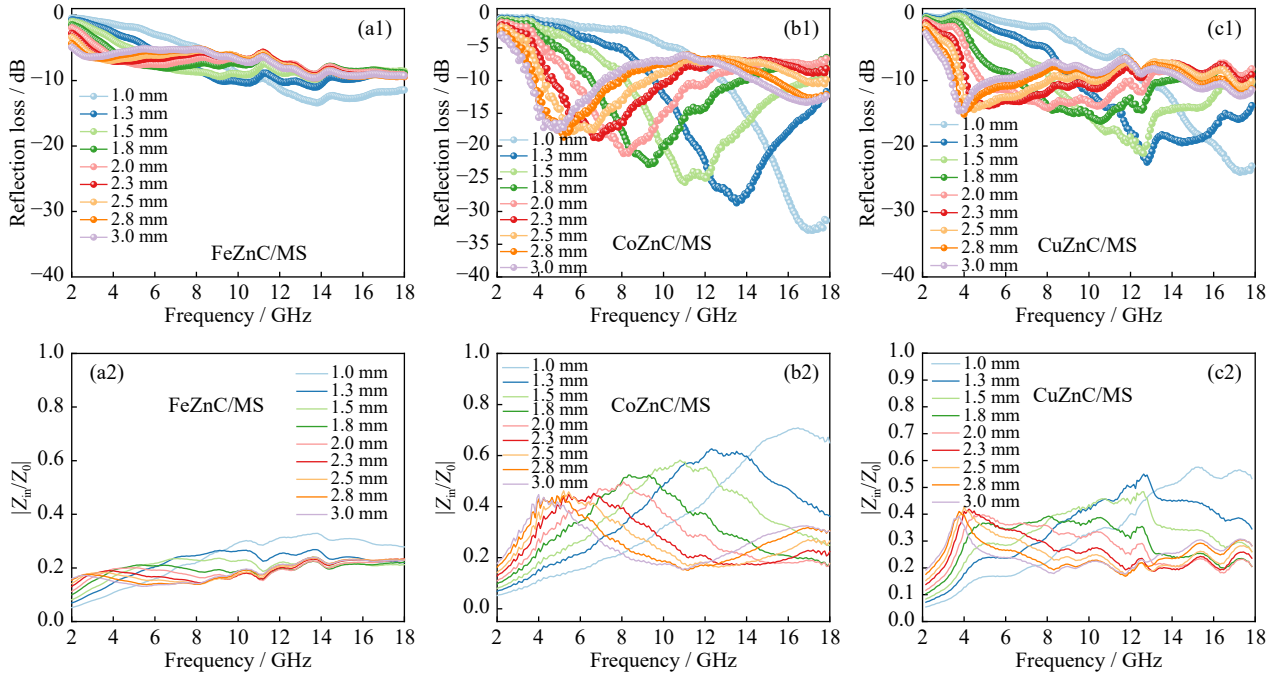

Fig. 8. (a1–c1) Frequency dependence of the RL curves and (a2–c2) input impedance matching $|Z_{in}/Z_0|$ for the FeZnC/MS, CoZnC/MS, and CuZnC/MS.

ization relaxation processes under an alternating current electric field (Fig. 9(a)–(c)).

When the external electric field disappears, the dipole is reoriented driven by thermal motion, which is a dipole polarization relaxation process. According to the Debye dipolar relaxation theory, the relationship between ε' and ε'' can be written as Eq. (3) [38]:

$$[\varepsilon' - (\varepsilon_s + \varepsilon_\infty)/2] + (\varepsilon'')^2 = [(\varepsilon_s - \varepsilon_\infty)/2]^2 \quad (3)$$

where ε_∞ and ε_s represent the relative and static dielectric constants, respectively. The Cole–Cole semicircle plot is used to describe the Debye relaxation process, composed of ε' and ε''. In heterojunction materials, interfacial polarization and its relaxation process often occur, which is an energy loss caused by the lag of dipole orientation polarization in the material behind the change of the electric field. With the shape of the semicircle is determined by the dielectric relaxation time of the material and the correlation coefficient between temperature and frequency. Each semicircle in the plot represents a stage of Debye relaxation.

The Cole–Cole curves of all the samples possess a long trailing tail, indicating the contribution of conductivity loss to the EMWA properties. In general, the attenuation of EMW in magnetic absorbers strongly depends on magnetic loss, including hysteresis loss, eddy current loss (C_0), natural resonance and exchange resonance [39]. For the prepared composites eddy current loss and natural resonance can be generated from 2–18 GHz.

In the new type of composite material combining carbon materials and magnetic materials, magnetic loss is mostly caused by C_0, which is closely related to the conductivity and thickness of the material. Under the action of an applied magnetic field, an induced current is generated inside the material, which leads to energy dissipation, known as eddy current loss. Therefore, by adjusting the above parameters of the material, the eddy current loss can be effectively controlled, thereby affecting the overall magnetic performance of the material. It can be expressed as Eq. (4) [40]:

$$C_0 = \mu''(\mu')^{-2} f^{-1} = 2\pi\mu_0 d^2\sigma \quad (4)$$

where μ_0 and σ represent the vacuum permeability and conductivity, respectively. If the value of C_0 remains constant with frequency, it means that eddy current losses account for the main contribution to the magnetic loss [41]. The C_0 curve of FeZnC/MS (Fig. 9(d)) fluctuates slightly in the range of 2–13 GHz and stabilize in the range of 13–18 GHz, which

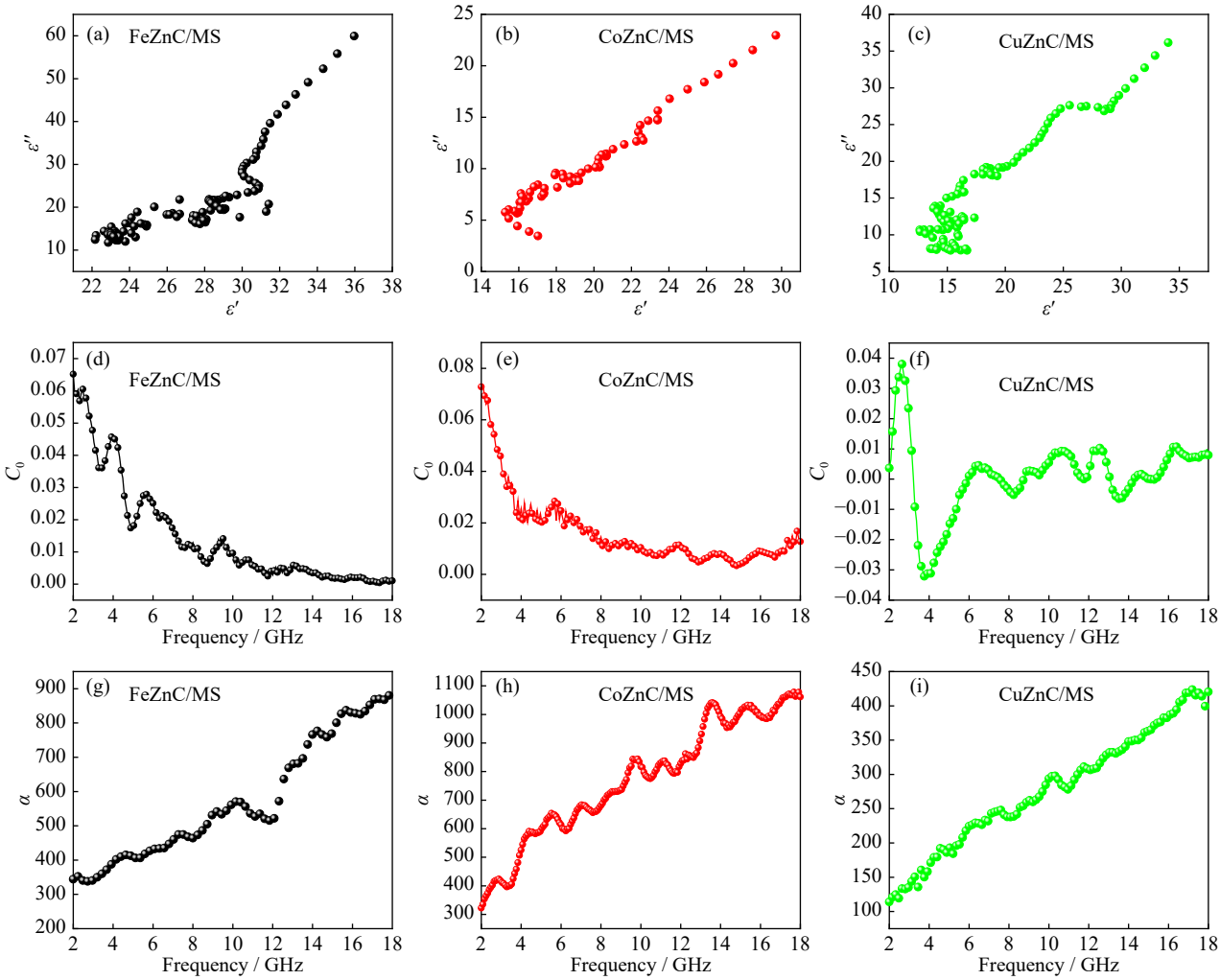

Fig. 9. (a–c) Cole–Cole curves, (d–f) eddy current loss, and (g–i) attenuation constant of FeZnC/MS, CoZnC/MS, and CuZnC/MS, respectively.

suggests that the main magnetic loss mechanisms of FeZnC/MS nanocomposites are natural resonance and eddy current loss in the range of 2–13 and 13–18 GHz, respectively. The C_0 curve of CoZnC/MS (Fig. 9(e)) decreases sharply in the range of 2–5 GHz and fluctuates in the range of 13–18 GHz, suggesting that natural resonance dominates the magnetic loss mechanism in the low and high frequency range. The C_0 curve of CuZnC/MS (Fig. 8(f)) fluctuates throughout the frequency, indicating that the natural resonance is mainly responsible for the magnetic loss.

The attenuation constant (α) of absorbing materials is generally used to describe the characteristics of absorbers in the process of absorbing and transmitting EMW. The lager α of the absorbing material, the higher its absorption and scattering effects on EMW, and it can better weaken the EMW energy. The α of absorbing materials can be described using the EM parameters, as shown in Eq. (5) [42]:

$$\alpha = \frac{\pi f \sqrt{2}}{c} \times \sqrt{\mu''\varepsilon'' - \mu'\varepsilon' + \sqrt{(\mu'\varepsilon'' + \mu''\varepsilon')^2 + (\mu''\varepsilon'' - \mu'\varepsilon')^2}} \quad (5)$$

The α value of all composites increases with increasing frequency. The largest α values of CoZnC/MS composite indicates that it exhibits a stronger electromagnetic wave attenuation capability. Table 1 summarizes the relevant parameters of Fe/Co/Cu-based EMW absorbers recently reported in the literature. It can be seen from the comparison that the prepared CoZnC/MS absorber combine the advantages of strong loss and wide absorption bandwidth, and show excellent EMWA performance.

According to the study shown in Fig. 10, the electromagnetic wave absorption mechanism of CoZnC 3D network-structured hollow MS carbon composites is mainly affected by the following factors: firstly, the unique hollow structure of the composites optimises impedance matching and triggers multiple reflections and scattering [52–58], which allows the EWM to propagate over long distances in the confined air space, and thus converts the energy into heat or other types of energy [59–68]. Secondly, CoZnC/MS has a large number of interfaces between them, leading to interfacial polarization, which results in the attenuation of EMW energy. Finally, based on the electromagnetic coupling effect, the attenuation of electromagnetic energy is increased by the synergistic loss of the dielectric (MS carbon) and magnetic (CoZnC) components, which leads to excellent EMWA properties.

Table 1. Recently reported Fe/Co/Cu-based EMW absorbers and related performance parameters

Sample	Thickness / mm	RL_{min} / dB	EAB / GHz	Ref.
FeNi/C	1.65	−40.20	5.50	[43]
Fe@C	3.00	−37.70	7.50	[44]
Fe/Co decorated C@CNTs	1.70	−24.83	5.14	[45]
rGO/Fe_3O_4	1.20	−33.00	3.00	[46]
C/Cu/NiP	1.70	−45.90	3.00	[47]
Fe/Fe_3O_4/biomass carbon	2.06	−30.41	2.45	[48]
Fe/C	2.50	−20.60	6.24	[49]
Co/$Co(OH)_2$@PCN	2.20	−25.80	7.10	[50]
$Co_{0.7}Fe_{0.3}$@C@void@C	2.11	−24.10	7.21	[51]
CoZnC/MS	1.20	−33.60	9.60	This work

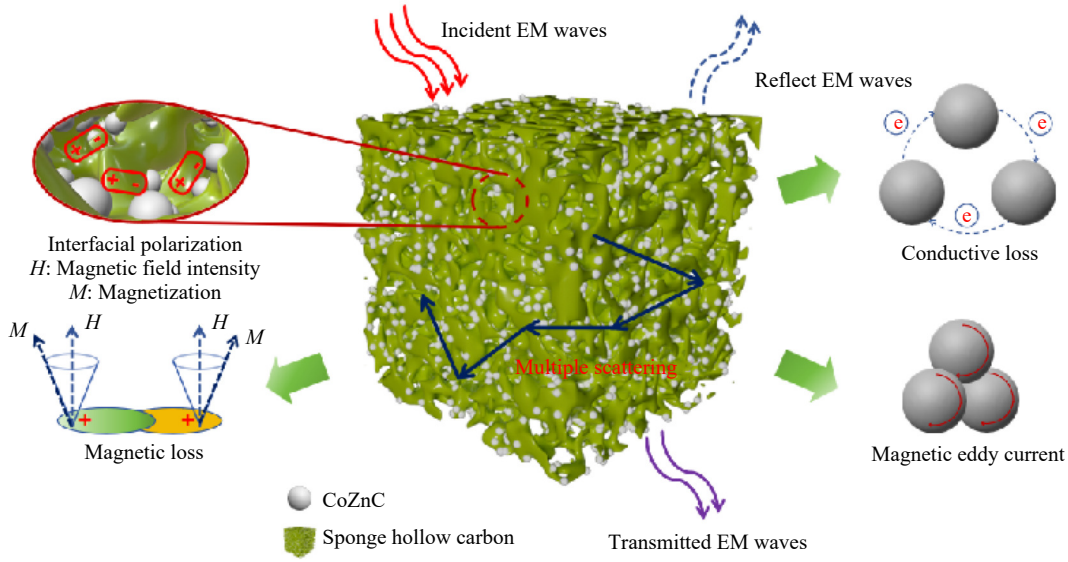

Fig. 10. EMW mechanism of CoZnC/3D network structure hollow MS carbon composite.

4. Conclusion

In this work, FeZnC/MS, CoZnC/MS and CuZnC/MS composites were successfully synthesized on the 3D framework MS by replacing Ni elements in $Ni_3ZnC_{0.7}$ with Fe, Co and Cu elements through the sol–gel method and immersion method, so that the composites were filled with Cu, Fe and Co particles and carbon nanotubes. Compared with Fe and Cu element substitution, the CoZnC composites have better EMWA performance, which can be attributed to the excel-

lent magnetic properties of Co and the dielectric properties of MS improving impedance matching, so that EMW can enter the material to be attenuated when the paraffin filling ratio is 1:1, the RL_{min} of the CoZnC/MS is −33.60 dB, and the EAB is 9.60 GHz, which is a significant improvement in EAB compared with $Ni_3ZnC_{0.7}$/MS. In addition, the effect of different paraffin filling rates of the materials on the performance of EMWA is investigated with bad EMWA performance after reducing the fill ratio. This work increases the magnetism of the composite by replacing weaker magnetic metals in the raw materials with stronger magnetic elements, optimizes impedance matching, and provides a new way for preparing high-performance absorbing materials.

Acknowledgements

This work was financially supported by the National Natural Science Foundation of China (Nos. 52101274, 52377026 and 52472131), Taishan Scholars and Young Experts Program of Shandong Province, China (No. tsqn202103057), Natural Science Foundation of Shandong Province, China (Nos. ZR2020QE011 and ZR2022ME089), the Qingchuang Talents Induction Program of Shandong Higher Education Institution, China (Research and Innovation Team of Structural-Functional Polymer Composites), Youth Top Talent Foundation of Yantai University, China (No. 2219008), Graduate Innovation Foundation of Yantai University, China (No. GIFYTU2240), College Student Innovation and Entrepreneurship Training Program Project, China (No. 202311066088).

Conflict of Interest

Guanglei Wu is an editorial board member for this journal and was not involved in the editorial review or the decision to publish this article. All authors do not have competing interests to declare.

Supplementary Information

The online version contains supplementary material available at https://doi.org/10.1007/s12613-024-3024-3.

References

[1] H.L. Lv, J.C. Cui, B.X. Li, M.Y. Yuan, J.J. Liu, and R.C. Che, Insights into civilian electromagnetic absorption materials: Challenges and innovative solutions, *Adv. Funct. Mater.*, (2024), art. No. 2315722.

[2] X.B. Xie, H.S. Wang, H. Kimura, C. Ni, W. Du, and G.L. Wu, NiCoZn/C@melamine sponge-derived carbon composites with high-performance electromagnetic wave absorption, *Int. J. Miner. Metall. Mater.*, 31(2024), No. 10, p. 2274.

[3] Y.H. Cheng, D. Lan, Z.R. Jia, *et al*., MOF derivatives anchored to multichannel hollow carbon fibers with gradient structures for corrosion resistance and efficient electromagnetic wave absorption, *J. Mater. Sci. Technol.*, 216(2025), p. 150.

[4] X.J. Zeng, C. Zhao, X. Jiang, R.H. Yu, and R.C. Che, Functional tailoring of multi-dimensional pure MXene nanostructures for significantly accelerated electromagnetic wave absorption, *Small*, 19(2023), No. 41, art. No. 2303393.

[5] N.X. Zhai, J.H. Luo, J. Mei, *et al*., Interface engineering of heterogeneous $NiSe_2$–$CoSe_2$@C@$MoSe_2$ for high-efficient electromagnetic wave absorption, *Adv. Funct. Mater.*, 34(2024), art. No. 2312237.

[6] Z.H. Zhou, D. Lan, J.W. Ren, *et al*., Controllable heterogeneous interfaces and dielectric modulation of biomass-derived nanosheet metal-sulfide complexes for high-performance electromagnetic wave absorption, *J. Mater. Sci. Technol.*, 185(2024), p. 165.

[7] Z.H. Zhou, X.F. Zhou, D. Lan, *et al*., Modulation engineering of electromagnetic wave absorption performance of layered double hydroxides derived hollow metal carbides integrating corrosion protection, *Small*, 20(2024), No. 8, art. No. 2305849.

[8] R.L. Liu, Y.K. Wang, P. Wang, *et al.*, *In situ* loading of $Ni_3ZnC_{0.7}$ nanoparticles with carbon nanotubes to 3D melamine sponge derived hollow carbon skeleton toward superior microwave absorption and thermal resistance, *Small*, 20(2024), No. 35, art. No. 2402438.

[9] S.J. Zhang, D. Lan, J.J. Zheng, *et al*., Rational construction of heterointerfaces in biomass sugarcane-derived carbon for superior electromagnetic wave absorption, *Int. J. Miner. Metall. Mater.*, 31(2024), No. 12, p. 2749.

[10] Y. Han, D. Lan, M.J. Han, Z.H. Xia, J.X. Zou, and Z.R. Jia, Construction of flower-like MoS_2 decorated on Cu doped CoZn-ZIF derived N-doped carbon as superior microwave absorber, *Nano Res.*, 17(2024), No. 9, p. 8250.

[11] L.H. Yu, G.J. Lian, G.Z. Zhu, *et al*., Hollow FeCoNiAl microspheres with stabilized magnetic properties for microwave absorption, *Nano Res.*, 17(2024), No. 3, p. 2079.

[12] B.L. Wang, C. Ni, X.B. Xie, M.C. Ding, and C.W. Li, Carbon nanotubes-encapsulated Co/Co_7Fe_3 nanocomposites: Achieving wideband electromagnetic wave absorption at ultrathin-thickness by regulating magnetic phase ratio, *Chem. Eng. J.*, 494(2024), art. No. 153076.

[13] S.J. Feng, R. Qiang, Y.L. Shao, *et al*., Fe_3C/Fe implanted hierarchical porous carbon as efficient electromagnetic wave absorber, *Diamond Relat. Mater.*, 149(2024), art. No. 111556.

[14] Z.Q. Xu, S. Wang, Y. Xie, *et al*., Monodisperse branched nickel carbide nanoparticles *in situ* grown on reduced graphene oxide with excellent electromagnetic absorption properties, *J. Alloys Compd.*, 900(2022), art. No. 163453.

[15] Q.G. Ren, T. Feng, Z. Song, *et al*., Autogenous and tunable CNTs for enhanced polarization and conduction loss enabling sea urchin-like Co_3ZnC/Co/C composites with excellent microwave absorption performance, *ACS Appl. Mater. Interfaces*, 14(2022), No. 36, p. 41246.

[16] J.H. Wen, D. Lan, Y.Q. Wang, *et al*., Absorption properties and mechanism of lightweight and broadband electromagnetic wave-absorbing porous carbon by the swelling treatment, *Int. J. Miner. Metall. Mater.*, 31(2024), No. 7, p. 1701.

[17] Y.P. Qi, Y.X. Yang, H.L. Sun, *et al*., Three-dimensional melamine sponge hollow carbon/$Ni_3ZnC_{0.7}$/carbon nanotubes with tunable high-performance microwave absorption performance, *Synth. Met.*, 295(2023), art. No. 117351.

[18] H. Ding, Z.H. Sun, S.Y. Tian, *et al*., Tailoring $Ni_3ZnC_{0.7}$/graphite heterostructure in N-rich laminated porous carbon nanosheets for highly efficient microwave absorption, *Ceram. Int.*, 49(2023), No. 19, p. 31763.

[19] X.Q. Sun, Y.K. Wang, H. Kimura, *et al*., Thermal stability of $Ni_3ZnC_{0.7}$: As tunable additive for biomass-derived carbon sheet composites with efficient microwave absorption, *J. Colloid Interface Sci.*, 642(2023), p. 447.

[20] C. Ni, D. Wu, X.B. Xie, *et al*., Microwave absorption properties of microporous CoNi@(NiO–CoO) nanoparticles through

dealloying, *J. Magn. Magn. Mater.*, 503(2020), art. No. 166631.
[21] P.F. Yin, Y.M. Luo, D. Lan, *et al*., Structural engineering of porous biochar loaded with ferromagnetic/anti-ferromagnetic $NiCo_2O_4$/CoO for excellent electromagnetic dissipation with flexible and self-cleaning properties, *J. Mater. Sci. Technol.*, 180(2024), p. 12.
[22] Y. Sun, Y.J. Wang, H.J. Ma, *et al*., Fe_3C nanocrystals encapsulated in N-doped carbon nanofibers as high-efficient microwave absorbers with superior oxidation/corrosion resistance, *Carbon*, 178(2021), p. 515.
[23] W. Feng, Y.M. Wang, Y.C. Zou, J.C. Chen, D.C. Jia, and Y. Zhou, ZnO@N-doped porous carbon/Co_3ZnC core–shell heterostructures with enhanced electromagnetic wave attenuation ability, *Chem. Eng. J.*, 342(2018), p. 364.
[24] H.H. Zhu, Q.Z. Jiao, R.R. Fu, *et al*., Cu/NC@Co/NC composites derived from core–shell Cu–MOF@Co-MOF and their electromagnetic wave absorption properties, *J. Colloid Interface Sci.*, 613(2022), p. 182.
[25] Y.C. Wang, A.A. Haidry, Y.J. Liu, *et al*., Enhanced electromagnetic wave absorption using bimetallic MOFs-derived TiO_2/Co/C heterostructures, *Carbon*, 216(2024), art. No. 118497.
[26] Z.M. Wei, Y.H. Liu, J. Ding, Q.Y. He, Q. Zhang, and Y.M. Zhai, Promoting electrocatalytic CO_2 reduction to CO via sulfur-doped Co–N–C single-atom catalyst, *Chin. J. Chem.*, 41(2023), No. 24, p. 3553.
[27] Z.Y. Dai, P. Wu, L.R. Xiao, *et al*., Non-stoichiometric $Ni_3ZnC_{0.7}$ carbide loading on melamine sponge-derived carbon for hydrogen storage performance improvement of MgH_2, *Rare Met.*, (2024): DOI: 10.1007/s12598-024-02943-y
[28] Q.J. Wang, J.N. Wang, Y.Z. Zhao, *et al*., NiO/$NiFe_2O_4$@N-doped reduced graphene oxide aerogel towards the wideband electromagnetic wave absorption: Experimental and theoretical study, *Chem. Eng. J.*, 430(2022), art. No. 132814.
[29] M. Bleija, O. Platnieks, J. Macutkevič, *et al*., Poly(butylene succinate) hybrid multi-walled carbon nanotube/iron oxide nanocomposites: Electromagnetic shielding and thermal properties, *Polymers*, 15(2023), No. 3, art. No. 515.
[30] B. Zhang, X.B. Xie, Y.K. Wang, *et al.*, *In situ* formation of multiple catalysts for enhancing the hydrogen storage of MgH_2 by adding porous $Ni_3ZnC_{0.7}$/Ni loaded carbon nanotubes microspheres, *J. Magnesium Alloys*, 12(2024), No. 3, p. 1227.
[31] H.L. Yang, Z.J. Shen, H.L. Peng, Z.Q. Xiong, C.B. Liu, and Y. Xie, 1D–3D mixed-dimensional MnO_2@nanoporous carbon composites derived from Mn-metal organic framework with full-band ultra-strong microwave absorption response, *Chem. Eng. J.*, 417(2021), art. No. 128087.
[32] C.H. Wang, L.S. Zong, N. Li, *et al*., Light-weight 1D heteroatoms-doped Fe_3C@C nanofibers for microwave absorption with a thinner matching thickness, *J. Alloys Compd.*, 885(2021), art. No. 160968.
[33] Y.J. Wang, Y. Sun, Y. Zong, *et al*., Carbon nanofibers supported by FeCo nanocrystals as difunctional magnetic/dielectric composites with broadband microwave absorption performance, *J. Alloys Compd.*, 824(2020), art. No. 153980.
[34] H. Zhao, Y.S. Huang, Y.C. Han, *et al*., Flexible and lightweight porous polyether sulfone/Cu composite film with bidirectional differential structure for electromagnetic interference shielding and heat conduction, *Chem. Eng. J.*, 440(2022), art. No. 135919.
[35] X.J. Chen, M.Z. Yang, X.S. Zhao, D.C. Hu, W. Liu, and W.S. Ma, Tailoring superhydrophobic PDMS/$CeFe_2O_4$/MWCNTs nanocomposites with conductive network for highly efficient microwave absorption, *Chem. Eng. J.*, 432(2022), art. No. 134226.
[36] N. Li, L.H. Liu, Y. Duan, *et al*., Exploration of magnetic media modulation engineering on heterogeneous carbon spheres for optimized electromagnetic wave absorption, *J. Alloys Compd.*, 943(2023), art. No. 169109.
[37] B. Wei, M.Q. Wang, Z.J. Yao, *et al*., Bimetallic nanoarrays embedded in three-dimensional carbon foam as lightweight and efficient microwave absorbers, *Carbon*, 191(2022), p. 486.
[38] M.X. Sun, W.Q. Cao, P.Y. Zhu, *et al*., Thermally tailoring magnetic molecular sponges through self-propagating combustion to tune magnetic-dielectric synergy toward high-efficiency microwave absorption and attenuation, *Adv. Compos. Hybrid Mater.*, 6(2023), No. 1, art. No. 54.
[39] Y. Li, X.F. Liu, X.Y. Nie, *et al*., Microwave absorbing materials: Multifunctional organic–inorganic hybrid aerogel for self-cleaning, heat-insulating, and highly efficient microwave absorbing material, *Adv. Funct. Mater.*, 29(2019), No. 10, art. No. 1807624.
[40] X.J. Zeng, C. Zhao, Y.C. Yin, *et al*., Construction of $NiCo_2O_4$ nanosheets-covered $Ti_3C_2T_x$ MXene heterostructure for remarkable electromagnetic microwave absorption, *Carbon*, 193(2022), p. 26.
[41] J.C. Sun, Z.D. He, W.J. Dong, W.H. Wu, and G.X. Tong, Broadband and strong microwave absorption of Fe/Fe_3C/C core–shell spherical chains enhanced by dual dielectric relaxation and dual magnetic resonances, *J. Alloys Compd.*, 782(2019), p. 193.
[42] P.B. Liu, Y. Wang, G.Z. Zhang, *et al*., Hierarchical engineering of double-shelled nanotubes toward hetero-interfaces induced polarization and microscale magnetic interaction, *Adv. Funct. Mater.*, 32(2022), No. 33, art. No. 2202588.
[43] R.W. Shu, N.N. Li, X.H. Li, and J.J. Sun, Preparation of FeNi/C composite derived from metal-organic frameworks as high-efficiency microwave absorbers at ultrathin thickness, *J. Colloid Interface Sci.*, 606(2022), p. 1918.
[44] Z.M. Deng, Y. Li, H.B. Zhang, *et al*., Lightweight Fe@C hollow microspheres with tunable cavity for broadband microwave absorption, *Composites Part B*, 177(2019), art. No. 107346.
[45] Y. Wang, Q.K. Man, S.Q. Zhu, Z.K. Lei, G.G. Tan, and H.T. Guan, Fe/Co decorated C@CNTs derived from bimetallic metal–organic-framework for microwave absorption with wide bandwidth, *J. Alloys Compd.*, 967(2023), art. No. 171645.
[46] S. Li, Y. Li, X. Han, X.R. Zhao, and Y. Zhao, High-efficiency enhancement on thermal and electrical properties of epoxy nanocomposites with core–shell carbon foam template-coated graphene, *Composites Part A*, 120(2019), p. 95.
[47] Y.P. Wei, Y.H. Yu, H.Y. Li, *et al*., The double-coating structure of C/Cu/NiP microfiber composites for enhanced microwave absorption properties, *J. Mater. Sci. Mater. Electron.*, 33(2022), No. 17, p. 14202.
[48] J.B. Su, R. Yang, P.K. Zhang, *et al*., Fe/Fe_3O_4/biomass carbon derived from agaric to achieve high-performance microwave absorption, *Diamond Relat. Mater.*, 129(2022), art. No. 109386.
[49] S.X. Dong, J. Li, N. Li, *et al*., Enhanced broadband microwave absorption of Fe/C core–shell nanofibers in X and Ku bands, *Ceram. Int.*, 49(2023), No. 5, p. 8181.
[50] Y.H. Wu, G.D. Wang, X.X. Yuan, G. Fang, P. Li, and G.B. Ji, Heterointerface engineering in hierarchical assembly of the Co/$Co(OH)_2$@carbon nanosheets composites for wideband microwave absorption, *Nano Res.*, 16(2023), No. 2, p. 2611.
[51] L.Z. Meng, J.H. Wang, J.Y. Qi, *et al*., Yolk–shell construction of $Co_{0.7}Fe_{0.3}$ modified with dual carbon for broadband microwave absorption, *J. Colloid Interface Sci.*, 659(2024), p. 945.
[52] M.J. Han, D. Lan, Z.M. Zhang, *et al*., Micro-sized hexapod-like CuS/Cu_9S_5 hybrid with broadband electromagnetic wave absorption, *J. Mater. Sci. Technol.*, 214(2025), p. 302.
[53] B.L. Wang, M.C. Ding, C.X. Shao, *et al*., Facile synthesis of Co_xFe_y@C nanocomposite fibers derived from pyrolysis of cobalt/iron chelate nanowires for strong broadband electromagnetic wave absorption, *Chem. Eng. J.*, 465(2023), art. No. 142803.

[54] Y.Y. Lian, D. Lan, X.D. Jiang, *et al*., Multifunctional electromagnetic wave absorbing carbon fiber/$Ti_3C_2T_X$ MXene fabric with superior near-infrared laser dependent photothermal antibacterial behaviors, *J. Colloid Interface Sci.*, 676(2024), p. 217.
[55] L.R. Xiao, Y.K. Wang, H. Kimura, *et al*., Synergetic dielectric and magnetic losses of melamine sponge-loaded puffed-rice biomass carbon and $Ni_3ZnC_{0.7}$ for optimal effective microwave absorption, *J. Colloid Interface Sci.*, 653(2024), p. 570.
[56] S.J. Zhang, D. Lan, J.J. Zheng, Z.W. Zhao, Z.R. Jia, and G.L. Wu, Insights into polarization relaxation of electromagnetic wave absorption, *Cell Rep. Phys. Sci.*, 5(2024), No. 9, art. No. 102206.
[57] L.L. Liang, W.H. Gu, Y. Wu, *et al*., Heterointerface engineering in electromagnetic absorbers: New insights and opportunities, *Adv. Mater.*, 34(2022), No. 4, art. No. 2106195.
[58] Z.Q. Guo, D. Lan, Z.R. Jia, *et al*., Multiple tin compounds modified carbon fibers to construct heterogeneous interfaces for corrosion prevention and electromagnetic wave absorption, *Nano Micro Lett.*, 17(2024), No. 1, art. No. 23.
[59] C.H. Sun, D. Lan, Z.R. Jia, Z.G. Gao, and G.L. Wu, Kirkendall effect-induced ternary heterointerfaces engineering for high polarization loss MOF–LDH–MXene absorbers, *Small*, 20(2024), No. 48, art. No. 2405874.
[60] Z.R. Jia, L.F. Sun, Z.G. Gao, and D. Lan, Modulating magnetic interface layer on porous carbon heterostructures for efficient microwave absorption, *Nano Res.*, 17(2024), No. 11, p. 10099.
[61] T.B. Zhao, D. Lan, Z.R. Jia, Z.G. Gao, and G.L. Wu, Hierarchical porous molybdenum carbide synergic morphological engineering towards broad multi-band tunable microwave absorption, *Nano Res.*, 17(2024), No. 11, p. 9845.
[62] Y.L. Zhang, K.P. Ruan, K. Zhou, and J.W. Gu, Controlled distributed $Ti_3C_2T_x$ hollow microspheres on thermally conductive polyimide composite films for excellent electromagnetic interference shielding, *Adv. Mater.*, 35(2023), No. 16, art. No. 2211642.
[63] G.J. Ma, D. Lan, Y. Zhang, *et al*., Microporous cobalt ferrite with bio-carbon loosely decorated to construct multi-functional composite for dye adsorption, anti-bacteria and electromagnetic protection, *Small*, 20(2024), No. 45, art. No. 2404449.
[64] J.M. Yang, H. Wang, Y.L. Zhang, H.X. Zhang, and J.W. Gu, Layered structural PBAT composite foams for efficient electromagnetic interference shielding, *Nano Micro Lett.*, 16(2023), No. 1, art. No. 31.
[65] Y. Liu, X.Y. Ren, X.F. Zhou, *et al*., Defect design and vacancy engineering of $NiCo_2Se_4$ spinel composite for excellent electromagnetic wave absorption, *Ceram. Int.*, 50(2024), No. 22, p. 46643.
[66] Z.Y. Shen, D. Lan, Y. Cong, Y.Y. Lian, N.N. Wu, and Z.R. Jia, Tailored heterogeneous interface based on porous hollow In–Co–C nanorods to construct adjustable multi-band microwave absorber, *J. Mater. Sci. Technol.*, 181(2024), p. 128.
[67] J. Jiang, D. Lan, Y.Q. Li, *et al*., Construction of spherical heterogeneous interface on $ZnFe_2O_4$@C composite nanofibers for highly efficient microwave absorption, *Ceram. Int.*, 50(2024), No. 20, p. 38331.
[68] Y. Zhang, J. Wang, Q.L. Wu, *et al*., Enhanced electromagnetic wave absorption of bacterial cellulose/reduced graphene oxide aerogel by eco-friendly *in situ* construction, *J. Colloid Interface Sci.*, 678(2025), p. 648.